Available online at www.sciencedirect.com

SciVerse ScienceDirect

Physics Procedia 36 (2012) 1195 – 1205

Physics Procedia

Superconductivity Centennial Conference

Simulation Setup for Modeling the Thermal, Electric, and Magnetic Behavior of High Temperature Superconductors.

Alexander Henning[a], Manfred Lindmayer[b], Michael Kurrat[b] a*

[a]*Technische Universität Braunschweig, Institut für Hochspannungstechnik und Elektrische Energieanlagen – now with Bruker ASC GmbH, Schleinitzstrasse 23, 38106 Braunschweig, Germany*

[b]*Technische Universität Braunschweig, Institut für Hochspannungstechnik und Elektrische Energieanlagen, Schleinitzstrasse 23, 38106 Braunschweig, Germany*

Abstract

This paper presents a new simulation setup for the calculation of high temperature superconductors. This setup incorporates the magnetic and electric field dependencies as well as the current and temperature dependencies on the electrical resistivity of high temperature superconductors. Multi-conductor arrangements and 3D models can be calculated, too. The implementation in the commercially available FEM software Comsol is shown together with the underlying equations used in the simulation setup together with some exemplary simulations.
Additionally, some interesting results regarding the penetration behavior of current density and electric field of high temperature superconductors are shown.

Keywords: superconductiviy; simulation; field penetration; fault current limiter;

1. Introduction

The electrical resistivity of high temperature superconductor materials depends on the parameters temperature, current density, and external magnetic field. One type of superconducting devices – the superconducting fault current limiters (FCL) is using these dependencies. Of these FCL – the inductive shielded fault current limiter [1] – utilizes the transition from the superconducting state to normal conducting state if the current exceeds the critical current of the superconductor during a fault to “switch” an inductance into the grid which limits the short circuit current. While the grid is operating normally,

* Corresponding author: Alexander Henning.
E-mail address: al.henning@tu-bs.de

1875-3892 doi:10.1016/j.phpro.2012.06.201

most of the inductance of the FCL is shielded by the superconductor, which is in its superconducting state. During a fault the current exceeds the critical current, causing a very rapid increase of the electrical resistivity and therefore a very rapid rise of the temperature too. During entire operation time the HTS material is exposed to the magnetic field of the primary coil of the inductive FCL. Therefore the quench process as well as the operation in its superconducting state (where the HTS should shield the magnetic field), is a complex interaction between the induced current flow in the superconductors. This interaction is influenced by the current density, magnetic flux density and temperature dependent resistivity, the temporal and local evolution of these values in high temperature superconductors (HTS), its substrate and the external circuit [2]. The design and optimization of HTS current limiters is therefore a costly and time-consuming process. It can be optimized by software tools able to describe the HTS and predict its behavior under different operational conditions. But the coupled dependencies of the electrical resistivity on temperature, current density, and magnetic flux are not implemented in present commercially available software. To avoid long term software development the commercially available FEA program Comsol® has been customized for the simulation of HTS materials. Additionally there are several effects like local and temporal temperature and current density distributions which are very hard to measure. To get new information about the behavior of HTS material, simulations can be a good tool.

2. Numerical method

2.1. Basic equations

For implementation into the FEM software Comsol the so called ***A***-*V* formulation [3, 4] was chosen. Here the magnetic flux density ***B*** and the electric field ***E*** are linked to the magnetic vector potential ***A*** and to an electric scalar potential *V* via:

$$\vec{B} = \nabla \times \vec{A} \tag{1}$$

and

$$\vec{E} = -\frac{\partial \vec{A}}{\partial t} - \nabla V \tag{2}$$

The material properties are described via the constitutive equations

$$\vec{B} = \mu \cdot \vec{H} \tag{3}$$

and

$$\vec{j} = \sigma \cdot \vec{E} \tag{4}$$

The starting point for the calculation of the distributions of magnetic fields and current densities in and around a conductor (not only a superconductor) is Ampere's law (1) and the current conservation law in differential form (2).

$$\nabla \times \left(\frac{1}{\mu} \nabla \times \vec{A} \right) = \vec{j} = \vec{j}_W + \vec{j}_V = -\sigma \left(\frac{\partial \vec{A}}{\partial t} + \nabla V \right) \tag{5}$$

$$\nabla \bullet \vec{J} = -\nabla \bullet \left[\sigma \left(\frac{\partial \vec{A}}{\partial t} + \nabla V \right) \right] = 0 \tag{6}$$

The overall current density consists of the eddy current density $\boldsymbol{j_W}$ and the "ohmic" current density $\boldsymbol{j_V}$ due to the potential gradient. This system of equations allows for the calculation of currents and magnetic fields in conductors with imposed voltages. If there are only induced currents, without predetermined electric potentials present, only the eddy current density exists, that means ∇V is zero and does therefore not apply.

The heat transfer in the simulations is expressed by the following equation:

$$\rho \cdot c \left(\frac{\partial T}{\partial t} \right) + \nabla \bullet \left(- [\lambda] \nabla T \right) = \ddot{q} \tag{7}$$

where ρ is the density, c the heat capacity, T the temperature, q the heat current density, $\ddot{q}$ the heat power density and $[\lambda]$ the thermal conductivity matrix. $\ddot{q}$ describes the heat generated per volume by ohmic losses in the model and can be expressed by:

$$\ddot{q} = \frac{\vec{j}^2}{\sigma} \tag{8}$$

$\boldsymbol{j}$ is the electrical current density and $\sigma = 1/\rho$ the electrical conductivity. The thermal parameters used in the simulations are: $\lambda = 6.1$ mW/(m*K), $\rho = 6.3$ kg/dm³ and $C_P = 0.16$ MJ/(kg*K). The initial temperature in the simulation is 77 K, the boiling point of liquid nitrogen.

These are the governing equations for the calculation of current densities, electric and magnetic fields, and heating in and around a conductor or superconductor. To implement the more special properties of HTS material some additional formulations are needed. These are shown in the next paragraph.

2.2. Model of HTS resistivity

To describe the thermal-electric characteristics of the specific resistivity of HTS material the following equation can be used. This equation is described in more detail in [5, 6]:

$$\rho(E,T) = \frac{\vec{E}}{J_C(T) \cdot \left(P \cdot \left(\frac{\vec{E}}{E_C} \right)^m + (1-P) \right)} \tag{9}$$

$\boldsymbol{E}$ is the electric field, E_C the electric field criterion (e.g. 1μV/cm); m and P are constants which are material-specific. $\rho(E)$ instead of $\rho(J)$ was used because of the FEM software used to avoid a circular dependency during the calculations. According to [7] the temperature dependent critical current density $J_C(T)$ can be written as:

$$J_C(T) = K \cdot \left(1 - \frac{T}{T_C}\right)^r$$
$$K = \frac{J_{C0,77K}}{\left(1 - \frac{77K}{T_C}\right)^r} \tag{10}$$

with r being a material parameter and T_C the critical temperature of the superconductor. But in this formulation no dependency of $\boldsymbol{B}$ is included yet; this can be done by using an additional equation for the critical current density [8-11] which is shown here:

$$J_C(B) = \frac{J_{C0}}{\left(1 + \frac{\sqrt{k_a^2 \vec{B}_{II}^2 + \vec{B}_{\perp}^2}}{B_0}\right)^{\beta}} \tag{11}$$

with the critical current density in self field J_{C0}, the anisotropy coefficient $k_a \leq 1$, the characteristic magnetic field B_0 and the field coefficient β.

The resistivity normal conducting range of the superconductor can be described by:

$$\rho(T) = \rho_0 \cdot \left(1 + \alpha \cdot \left(T - T\right)\right) \tag{12}$$

with ρ_0 being the resistivity at the reference temperature T_0, T is the temperature and α the temperature coefficient. According to [2] typical values for YBCO are: α = 9e-9 Ωm/K, ρ_0 = 3e-7 Ωm and T_0 = 0 K were used in the calculations shown in this paper.

Since Comsol uses the electric conductivity σ for calculation, (9) must be rewritten using $\sigma = 1/\rho$. (9)-(12), resulting in:

$$\sigma(E,T,B) = \frac{J_{C0} \cdot J_C(T) \cdot J_C(\vec{B}) \cdot \left(P \cdot \left(\frac{\vec{E}}{E_C}\right)^m + (1-P)\right)}{\vec{E}} + \frac{1}{\rho_0 \cdot (1 + \alpha(T - T_0))} \tag{13}$$

which was used for the simulations shown in this paper: The parameters used in the simulations were: m = 1/3, P = 0.033, E_C = 1μV/cm ,J_{C0} = 1e8 A/m² or 1e10 A/m², T_C = 88 K, r = 1,65, B_0 = 0,1 T, k_a = 1, β = 1 α = 9e-9 Ωm/K, ρ_0 = 3e-7 Ωm and T_0 = 0 K, which are typical values for YBCO thin films [4, 10]. A possible physical interpretation of the parameters can be found in [4]. For numerical reasons $\boldsymbol{E}$ (or $\partial \vec{A} / \partial t$ using (2)) must not be zero. This can be done by adding a small value. This defines practically an upper boundary to the electrical conductivity. In the simulations shown in this work a value of 1e-8 was used, which results in a maximal conductivity of σ = 6.667e15 S/m and is a good compromise between accuracy and computing time. Successful test simulations were made with values up to 1e-30, which results in maximal conductivity of $\sigma \approx$ 1e40 S/m but need very long computing times.

A comparison of the E-J characteristics of (13) with the widely used power law (14) [3, 4, 15, 16, 17] is shown in Fig. 1

$$\frac{|\vec{E}|}{E_C} = \left(\frac{|\vec{j}|}{J_C}\right)^n \tag{14}$$

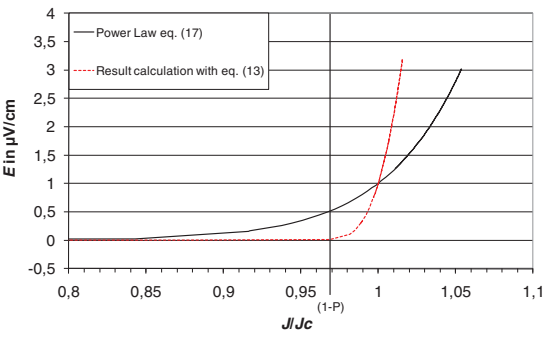

Fig. 1 Comparison of the *E-J* characteristics of the widely used power law (eq. (14)) and the formulation after eq. (13) with $J_C(B) = 1$, T = const =77 K at a point on the boundary of the superconductor. The exponent used in the power law formulation was $n = 30$.

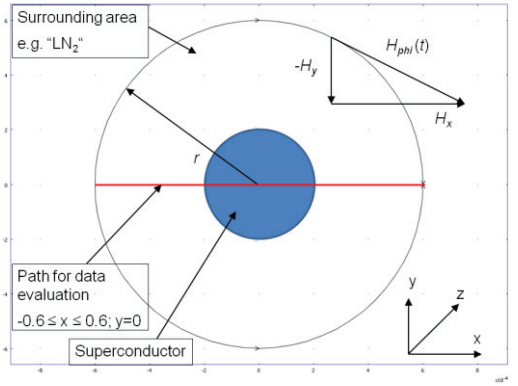

Fig. 2 Boundary conditions and round superconductor model used in this work.

The curves shown in Fig. 1 are from simulations based on the respective equations and were evaluated at a point on the boundary of the superconductor ($x = 0.2$; $y = 0$) from $t = 0$ to $t = 5$ ms. A comparison between the two formulations shows, that (13) makes a much better fit to the Bean model than the power law formulation according to (14). The exponent used in the simulation with the power law was $n = 30$. Additionally the Material dependent fit parameter m and P are temperature independent as shown in [6]. This makes it easier to implement (13) into FEM software.

2.3. Boundary conditions and simulation model

Fig. 2 shows a model of a round superconductor (blue area) with a surrounding area, which represents a LN_2 bath. The diameter of the superconductor in the model is 0.4 mm, the diameter of the outer area 1.2 mm, additionally the path used for data evaluation is shown.

The current flowing in the conductor was modeled as a boundary condition using the magnetic field $\boldsymbol{H}$. This can be done, because every current flow in a conductor results in a magnetic field around the conductor. Conversely it is therefore possible to describe the current in the conductor by defining the magnetic field $\boldsymbol{H}$ on the outer surface of the superconductor. This can be done by using the "magnetic field" boundary condition in Comsol, thus defining the magnetic field at the outer boundary of the model. Using a Cartesian coordinate system this magnetic field can be defined by the equations (15-16) where $\boldsymbol{H_{phi}}$ in (15) is the tangential magnetic field strength, and $\boldsymbol{H_x}$ and $\boldsymbol{H_y}$ the respective components (Fig. 2).

$$\vec{H}_{phi} = \frac{I}{2 \cdot \pi \cdot r} \tag{15}$$

$$\vec{H}_x = -\vec{H}_{phi} \cdot \frac{y}{r} \tag{16}$$

$$\vec{H}_y = \vec{H}_{phi} \cdot \frac{x}{r} \tag{17}$$

I is the current in the conductor, r the radius, and x and y are the local coordinate points. By using this formulation it is even possible to use additional external magnetic fields, that is fields not generated by the transport currents, simply by adding a fixed value or a value-function to $\boldsymbol{H}_x$ or $\boldsymbol{H}_y$. These boundary conditions are based on tutorial models of the Comsol software suite [13, 14].

The calculations shown in this paper are 2D, which means no change in z-direction is considered. Successful test calculations with simple 3D-models were also made, but because of the extremely long computing times no extensive simulations were made.

Cooling by liquid nitrogen (LN_2) was unaccounted for in the simulations shown in this work, to reduce the complexity of the model and thus the computing times. In the FEM software Comsol such cooling can be done e.g. by using a negative heat source on the outer boundary of the model which uses the boiling curve of LN_2 as underlying function.

3. Simulation results

The following section shows some simulation results using the described method. To obtain these results a stepwise approach was used. At first calculations at constant temperature without magnetic flux dependency are shown, secondly the temperature dependency is included and last the magnetic field dependency is included as well.

3.1. Simulations $\sigma(E,T=const.)$

At first simulations at constant temperature (77 K) without $J_C(B)$ dependency were made as a proof of concept of the simulation setup.

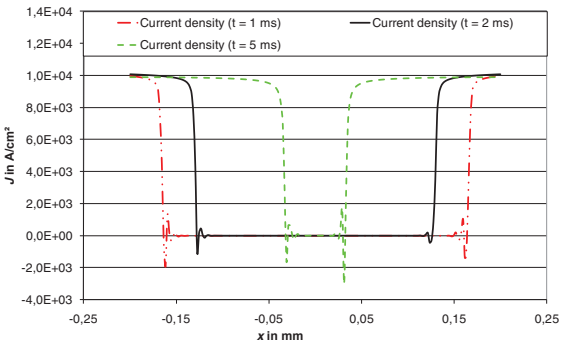

Fig. 3 Current density along the path for data evaluation (cf. Fig. 2) through the superconductor at different times. With an sinusoidal transport current $I = 0.95I_C$; $f = 50$ Hz.

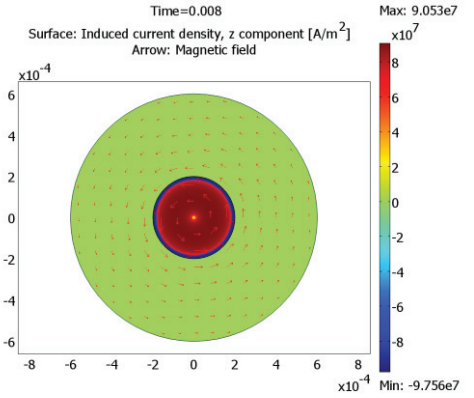

Fig. 4 Current density distribution in the simulation model at $t = 8$ms. The colors represent the current density, the arrows the magnetic field $\boldsymbol{H}$.

Fig. 3 shows the current density along the path for data evaluation shown in Fig. 2 at different times. The transport current used in this simulation was a 50 Hz sinusoidal current with $I = 0.95I_C$. It can be seen, that the current density penetrates the superconductor with an amplitude equal to J_C and penetrates deeper with rising transport current, which is to be expected for a superconductor. Fig. 4 shows the distribution of the current density in the same model at $t = 8$ ms. The positive half cycle (red color) has nearly fully penetrated the superconductor, the blue ring at the boundary shows the penetration of negative half cycle. Since the transport current during this calculation was only $0.95I_C$ a small area in the

middle of the superconductor stayed free of current density. These results show a good conformance with the Bean model, which proves that the simulation scheme works correctly.

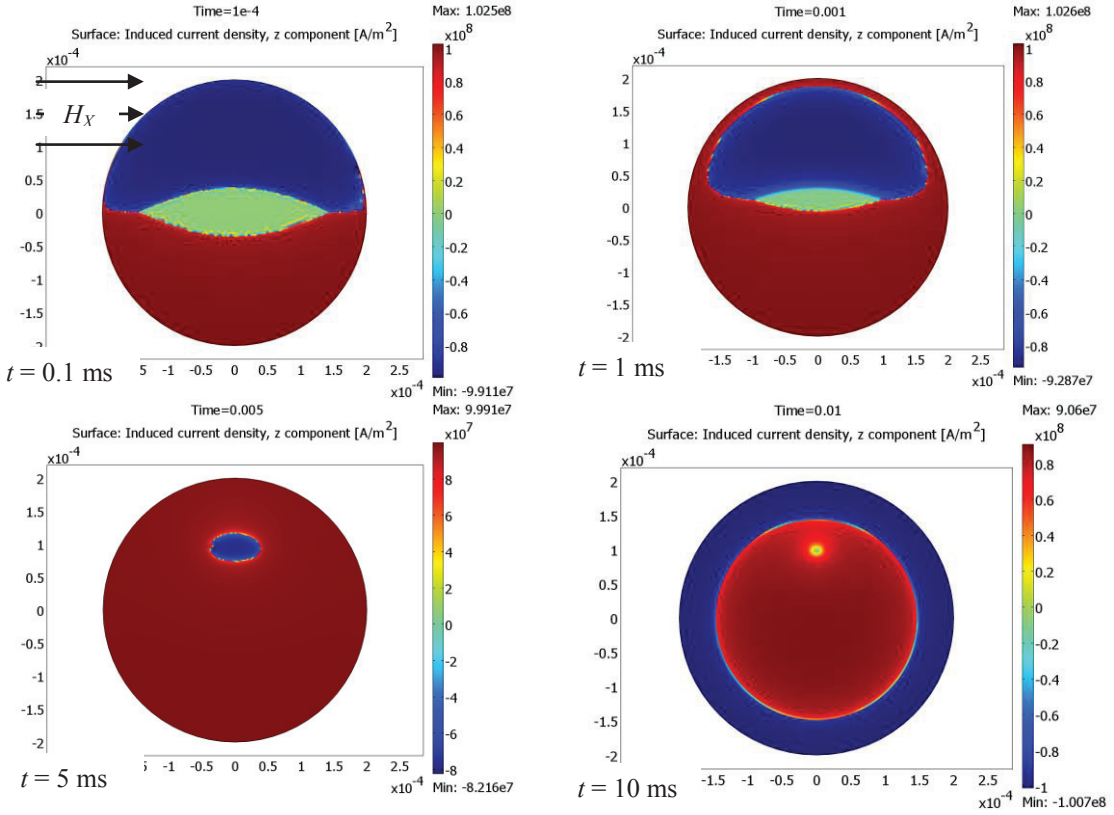

Fig. 5 Simulation with sinusoidal transport current (I = 0,95IC, f = 50 Hz) and an external magnetic field ($\boldsymbol{H_x}$ = 10 kA/m with μr = 1 $\boldsymbol{B_x}$ = 12.57 mT) at different times. For a better visibility the area around the superconductor is not shown.

It is possible to include external magnetic field into the simulations, too. Fig. 5 shows the current distribution in the conductor at different times. At t = 0.1 ms, the current density distribution induced by the external DC field where the transport current is still negligible is visible. With rising transport current the current density of the transport current superimposes the current density from the external magnetic field, which can be seen in the other times steps (t = 1, 5 and 10 ms) in Fig. 5.

3.2. Simulations σ(E,T)

The next step is the implementation of the temperature dependency of the critical current density into the simulation setup. This was done by using (10) for the characteristic of $J_C(T)$ as described in [6] and [7].

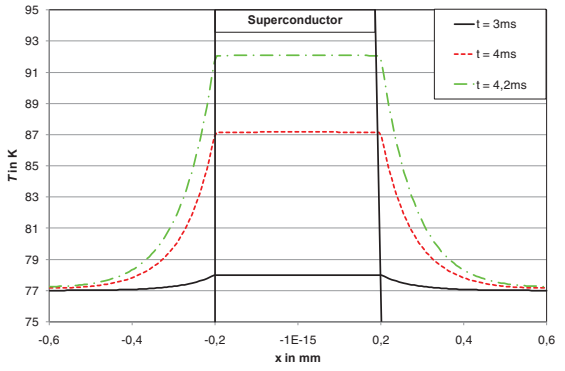

Fig. 6 Temperature in the simulation model along a path for data evaluation at different times (cf. Fig. 2).

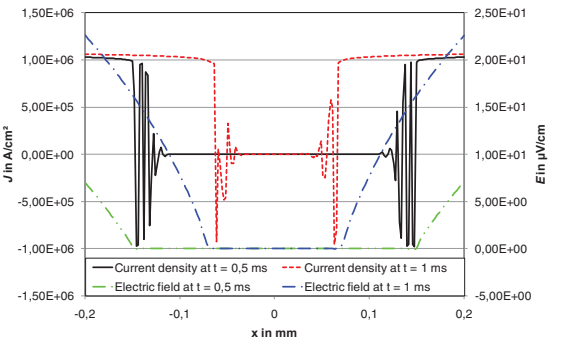

Fig. 7 Current density and electric field along a path for data evaluation (cf. Fig. 2) through the superconductor at different times.

Fig. 6 shows the temperature along the path for data evaluation (cf. Fig. 2) through the simulation model, while Fig. 7 shows the current density and the electric field along this path. The transport current used in these calculations was again a 50 Hz sinusoidal current with $I = 3I_C$. The oscillations visible in Fig. 7 are numerical artifacts and are resulting from the steep $\sigma(E,T)$ dependency in the simulation. They can be minimized by using smaller time steps and/or a finer finite-element mesh. But these measures lead to much longer computing times.

An interesting result is that the current density starts to penetrate the superconductor with higher values than J_C. More explicit this behavior is shown in Fig. 8, where the electric field and the current density at a point on the boundary of the superconductor are shown. In this simulation a ramped transport current was used, which followed the function:

$$I = I_0 \cdot \left(1 - \exp\left(\frac{t}{\tau}\right)\right) \qquad (18)$$

with $I_0 = I_C$ and $\tau = 10\mu s$.

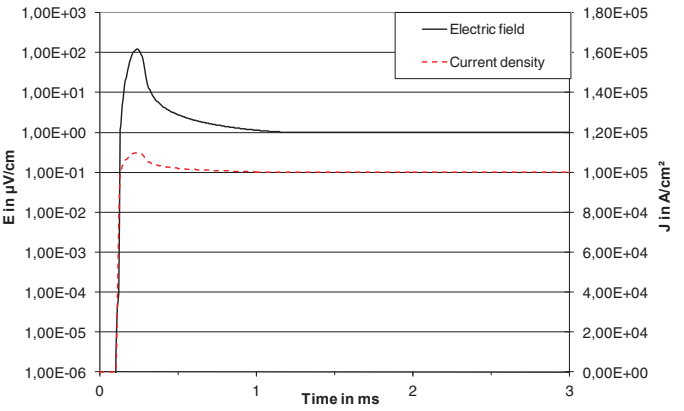

Fig. 8 Current density and electric field at a point on the boundary of the superconductor with a ramped transport current $I = I_C$.

A macroscopic explanation (without consideration of microscopic processes) of this behavior could be the following: With rising transport current the current density starts to penetrate the superconductor, but because of the self inductance of the conductor this penetration is not infinitely fast. Therefore the local current density at the boundary of the superconductor will rise above the "critical current density", which is defined as a certain point in the *E-J* characteristic (13). According to eq. (4) and (13) this leads to a local electric field much higher than the critical field E_C. The penetration of the current density is thus a current commutation, whose velocity depends on the inductivity/resistivity (L/R) ratio of the conductor. The local and temporal current distribution is therefore defined by the partial differential equations used in the calculation.

At longer times this redistribution of the current density is proceeding further till the current density reaches its DC-value everywhere in the superconductor. This equalization happens because of the finite electrical conductivity in the simulated superconductor, which is necessary for numerical reasons (cf. section 2.2). To stop the penetration of the current density in the superconducting state an infinite electrical conductivity would be needed.

3.3. Simulations $\sigma(E,T,B)$

Including the dependency on the magnetic flux density into the simulation setup was done using (11). This results in using (13) as shown in this paper in the FEM software, making it possible to simulate a superconductor including the field penetration with respect to the influence of all critical values ***J***, ***B***, and *T*. Fig. 9 shows the current density and magnetic flux density along the path shown in section 2.3 while using $\sigma(E,B,T)$ with an sinusoidal transport current at 50 Hz.

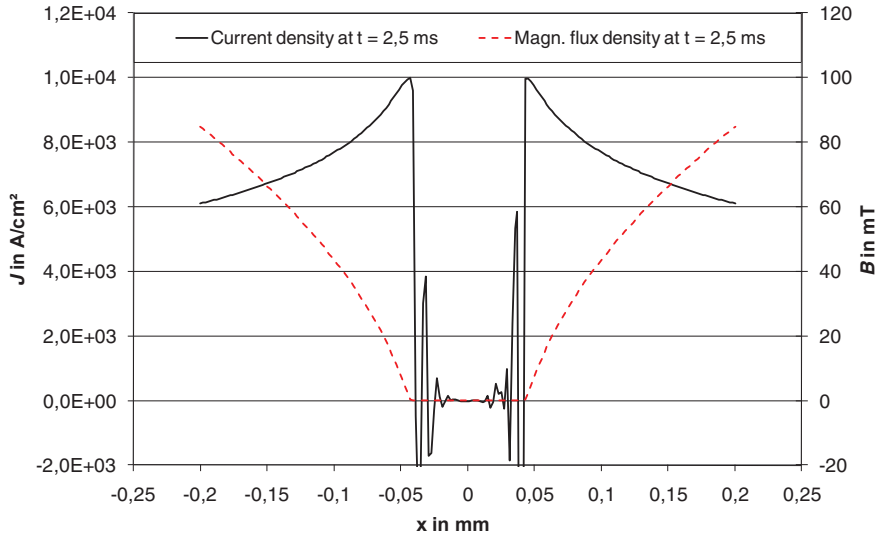

Fig. 9 Current density and magnetic flux density along a path for data evaluation (cf. Fig. 2) through the superconductor with a sinusoidal transport current with $I = I_C$ and $f = 50$ Hz; $J_C = 1e8$ A/m².

These curves follow the theoretically expected progression as seen for example in [19]. Because of the magnetic flux dependency, J_C is lowered in the regions with higher flux (boundary of the conductor) resulting in a lower amplitude of the penetrating current density.

3.4. Multi conductor arrangements

For the simulation of more application-oriented geometries it is often necessary to calculate several conductors with different transport currents flowing in each one. This can be done by the simulation setup shown in this work, by changing some of the boundary conditions. In detail the transport current is now defined by a potential difference ΔV along the length l (in z-direction) of each conductor. For 2D simulations this results in (20) for the current density in the conductor:

$$j = \sigma \cdot \left(\frac{\partial \vec{A}}{\partial t} + \frac{\Delta V}{l} \right) \tag{20}$$

The potential difference V is at first unknown, but comes out of the computation method by itself. In Comsol this can be done by additional algebraic equations, so called "Global equations".

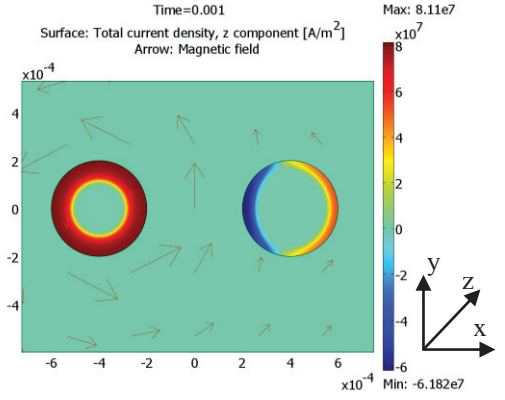

Fig. 10 Current density (colors) and magnetic field (arrows) in a 2-conductor model. The transport currents in this model were left conductor $I_1 = 0.5I_C$ (left conductor) and $I_1 = 0$ (right conductor).

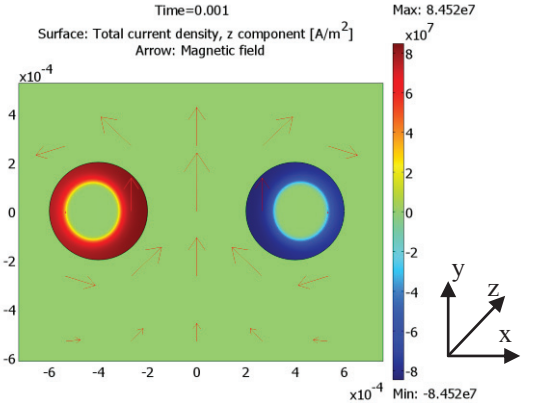

Fig. 11 Current density (colors) and magnetic field (arrows) in a 2-conductor model. The transport currents in this model were left conductor $I_1 = 0.5I_C$ (left conductor) and $I_1 = -0.5I_C$ (right conductor).

Fig. 10 shows a 2-conductor model with a ramped transport current $I_1 = 0.5I_C$ (left conductor) according to (18) and $I_1 = 0$ in the right conductor. In Fig. 11 the same model with the transport currents $I_1 = 0.5I_C$ and $I_1 = -0.5I_C$. In both models the surrounding area which represents LN_2 is not fully shown.

For the calculation of two conductors with independent transport currents, the following steps must be taken in detail:

- The electric field in eq. (13) is expressed by $\vec{E} = \left(\partial \vec{A} / \partial t + \Delta V / l\right)$.
- Two transport currents I_{01} and I_{02} must be defined.
- The unknown potential V_1 and V_2 are assigned to the respective conductor.
- The momentary currents I_1 and I_2 are calculated during the simulation by integration of the current density over the cross section of the conductor, by using the "Integration coupling variable" in Comsol.
- V_1 and V_2 are defined by two additional equations: $V_1 = I_1 - I_{01}$ und $V_2 = I_2 - I_{02}$ (Comsol: "Global equations"). The effect of these equations is that the potentials V_1 and V_2 adjust themselves in such a way that at each time $I_1 - I_{01} = 0$ and/or $I_2 - I_{02} = 0$ is valid.

3.5. Conclusions

A simulation scheme together with the underlying equations is shown, which allows simulating superconductors with respect to all critical values: Magnetic flux density $\boldsymbol{B}$, electrical current density $\boldsymbol{J}$, and temperature T. Additionally, the field penetration behavior of superconductors can be calculated along with the local and temporal field distributions in the superconductor. Multi-conductor arrangements can be simulated, too, as well as the losses inherent in superconductors.

The penetration of the current density into the conductor from outside is a dynamic process, which starts with current densities above the steady-state values, coinciding with a strongly increased initial voltage drop. This penetration is a current commutation, whose velocity depends on the inductivity/resistivity (L/R) ratio of the conductor.

Acknowledgements

The authors would like to thank colleagues of the Institut für Oberflächentechnik of the Technische Universität Braunschweig, the PerCoTech AG as well as the Siemens AG CT T DE HW 4 for help. The help of the COMSOL support is greatly acknowledged.

References

1. References

[1] Noe, Steurer, *Supercond. Sci. Technol.* **20,** 2007, R15-R29
[2] Gömöry, et.al. AC losses in coated conductors, *Supercond. Sci. Technol.* **23,** 2010
[3] Hofman C, Ries G, Modelling the interactions between magnets and granular high-Tc superconductor material with a finite-element method, *Supercond. Sci. Technol. 14*, **34-40, 2001**
[4] Bíró O, Preis K, On the use of the magnetic vector potential in the finite element analysis of three-dimensional eddy currents, *IEEE Trans. Magn. 25*, **3145-59, 1989**
[5] Grundmann J, et.al., Simulations of HTS switching with the finite element analysis program ANSYS. *Supercond. Sci. Technol. 16*, **No. 5 (May 2003)**, p562-565, 2003
[6] Henning, A, Grundmann, J, Kurrat, M, *J. Phys.: Conf. Ser.* **234,** 032021
[7] Prester, Current Transfer and Initial Dissipation in High-Tc-Superconductors, *Supercond. Sci. Technol.* **10 (333)**, 1998
[8] Gömöry, Improvement of the self-field critical current of a high-T_c superconducting tape by the edge cover from soft ferromagnetic material, *Appl. Phys. Lett.* **89**, 072506, 2006
[9] Gömöry *et al* 2008 *J. Phys.: Conf. Ser.* **97** 012096
[10] Gömöry, et.al., Magnetic flux penetration and AC loss in a composite superconducting wire with ferromagnetic parts, *Supercond. Sci. Technol.* **22** ,2009
[11] Gömöry, et.al. AC losses in coated conductors, *Supercond. Sci. Technol.* **23,** 2010
[12] Mosebach H, *Schaltverhalten von Hochtemperatur-Supraleiter-Bändern zur Strombegrenzung.* Shaker Verlag, Aachen, 1999
[13] Comsol AC/DC Module Library, *General Industrial Application Models, Superconducting Wire,* Version: November 2008, Comsol 3.5a
[14] Comsol Multiphysics tutorial model: "Skin Effect in a Circular Wire", Version: November 2008, Comsol 3.5a
[15] Ishii H, *et.al.*, Numerical approach for a description of electromagnetic phenomenon in superconducting composites, Advances in Superconductivity, vol. X, 1998
[16] Lehtonen J, *et.al.*, Computational comparison of magnetisation losses in HTS solenoids wound of tape conductors having different aspect ratios, *Supercond. Sci. Technol.* **12,** 1999
[17] Nibbio N, *et.al.*, Global properties of HTS tape model using field dependent power law in finite-element method, *Proc. Eucas, 1999*
[18] *Bean*, Phys. Rev. Lett. 8, 250, 1962
[19] Komarek, *Hochstromanwendungen der Supraleitung,* Teubner Stuttgard, 1995, ISBN 3-519-03225-2